Journal of Hydrology X 16 (2022) 100130

Contents lists available at ScienceDirect

Journal of Hydrology X

journal homepage: www.sciencedirect.com/journal/journal-of-hydrology-x

Research papers

Changes in extreme daily precipitation over Africa: Insights from a non-asymptotic statistical approach

Francesco Marra *, Vincenzo Levizzani, Elsa Cattani

Institute of Atmospheric Sciences and Climate, National Research Council of Italy (CNR-ISAC), Bologna 40129, Italy

ARTICLE INFO

This manuscript was handled by Marco Borga, Editor-in-Chief

ABSTRACT

Extreme precipitation heavily affects society and economy in Africa because it triggers natural hazards and contributes large amounts of freshwater. Understanding past changes in extreme precipitation could help us improve our projections of extremes, thus reducing the vulnerability of the region to climate change. Here, we combine high-resolution satellite data (1981–2019) with a novel non-asymptotic statistical approach, which explicitly separates intensity and occurrence of the process. We investigate past changes in extreme daily precipitation amounts relevant to engineering and risk management. Significant ($\alpha = 0.05$) positive and negative trends in annual maximum daily precipitation are reported in ~20 % of Africa both at the local scales (0.05°) and mesoscales (1°). Our statistical model is able to explain ~90% of their variance, and performs well (72% explained variance) even when annual maxima are explicitly censored from the parameter estimation. This suggests possible applications in situations in which the observed extremes are not quantitatively trusted. We present results at the continental scale, as well as for six areas characterized by different climatic characteristics and forcing mechanisms underlying the ongoing changes. In general, we can attribute most of the observed trends to changes in the tail heaviness of the intensity distribution (25% of explained variance, 38% at the mesoscale), while changes in the average number of wet days only explain 4% (12%) of the variance. Low-probability extremes always exhibit faster trend rates than annual maxima (~44% faster, in median, for the case of 100-year events), implying that changes in infrastructure design values are likely underestimated by approaches based on trend analyses of annual maxima: flexible change-permitting models are needed. No systematic difference between local and mesoscales is reported, with locally-varying impacts on the areal reduction factors used to transform return levels across scales.

1. Introduction

Africa is highly vulnerable to climate change due to its high socio-economic sensitivity to extreme weather events (Di Baldassarre et al., 2010; Liu et al., 2020; WMO, 2021). Extreme precipitation heavily affects society and economy because it triggers devastating natural hazards, such as floods and landslides (Nka et al., 2015; Igwe, 2018; Tramblay et al., 2020), and provides large amounts of freshwater to replenish groundwater resources (Samuels et al., 2009; Taylor et al., 2013). Quantifying and understanding past changes in extreme precipitation in Africa is thus of burning interest, because it helps improving our projections for engineering applications and risk and water resources management.

According to the last Intergovernmental Panel on Climate Change Assessment Report (IPCC: Climate Change, 2021) only two African regions, i.e., western and eastern South Africa, exhibit increasing trends in heavy precipitation attributable to the human contribution since the 1950s, although with a low confidence due to limited agreement. Due to the lack of long-term in-situ observations (Washington et al., 2006; Kidd et al., 2017), detection and attribution of trends in extreme precipitation in Africa proves rather uncertain, with sometimes contrasting results even for what concerns the direction of change (Cattani et al., 2018; Harrison et al., 2019). Nevertheless, numerous observational studies contribute to drawing the picture of heavy precipitation trends in Africa, typically examining high percentiles in the daily precipitation distribution (e.g., the 99th wet-day percentile) or the annual maximum daily amounts (RX1day or RX1), as detailed in the following.

One of the most investigated regions is Sahel-West Africa, where many works reported a recovery in the precipitation amounts and heavy precipitation since the 1980s, after decades of shortage, probably caused

* Corresponding author.
E-mail address: f.marra@isac.cnr.it (F. Marra).

https://doi.org/10.1016/j.hydroa.2022.100130
Received 2 March 2022; Received in revised form 7 July 2022; Accepted 10 July 2022
Available online 19 July 2022

by an increased intensity and frequency of mesoscale convective systems (e.g., Taylor et al., 2017; Nicholson et al., 2018; Vischel et al., 2019; Diatta et al., 2020; Chagnaud et al., 2021). Similarly, increasing precipitation amounts characterize western South Africa, particularly in the southern interior (Kruger and Nxumalo, 2017). Conversely, rainfall amounts decreased significantly in the Horn of Africa (Tierney et al., 2015), especially during the March-May rain season. This was likely caused by natural multidecadal variability of the tropical Pacific sea surface temperatures (Lyon 2014) or by a human-induced increase in the Indian Ocean sea surface temperatures, which modulates the Warm Pool circulation (Williams and Funk, 2011). Statistically significant negative trends in precipitation amount and number of wet days in autumn were recently found over the east, central and north-eastern parts of South Africa (MacKellar et al., 2014; Kruger and Nxumalo, 2017). Central Africa experienced a significant decrease in total precipitation, which is likely associated with a significant decrease of the length of the maximum number of consecutive wet days (Aguilar et al., 2009). Here, the area of the Congo basin, one of the world's most active thunderstorm regions where the second largest rainforest is situated, is witnessing a widespread increase in the boreal summer (June–August) dry season length since the 1980s (Jiang et al., 2019).

Given the poor and uneven spatial coverage of monitoring stations over Africa, it was difficult to infer an overall significant trend in RX1 and RX5 (the annual maxima at five consecutive days) (Westra et al., 2013; Sun et al., 2021). Nevertheless, it was possible to detect a predominance of positive trends for both indices from 1950 to 2018 in South Africa, where many ground stations are located (Westra et al., 2013). Similarly, positive trends were reported for Kenya and western Ethiopia based on geostationary satellite observations, and negative trends for eastern Ethiopia (Gebrechorkos et al., 2019). At a pan-African level, statistically significant positive trends in the annual averages of the monthly maxima from the Rainfall Estimates on a Gridded Network (Contractor et al., 2020) were reported during 1980–2016 in West and East Africa, whereas negative and non-significant deviations characterize southern Africa (Robinson et al., 2021).

Less is known about the changes in rarer extremes such as the amounts exceeded on average once in N years (termed N-year events or *return levels*), which are fundamental for engineering and risk management applications, and on the mechanisms behind these changes. The direct quantification of extreme return levels requires data series several times longer than the exceedance probability timescale; hence, statistical extrapolation models need to be used, such as extreme value distributions (Coles, 2001). These models rely on the observed extremes, either the annual maxima or the values exceeding very high thresholds, and require relatively long records to achieve a reasonable accuracy (Katz et al., 2002). Despite being preferable to traditional trend detection techniques (Zhang et al., 2004), quantifying changes between two periods is subject to large uncertainties because the temporal slices are usually short (Paeth et al., 2017). For example, De Waal et al. (2017) compared 50-year return levels from 76 rainfall stations in Western Cape (South Africa) estimated during 1980–2009 with those estimated during 1950–1979, finding an increase in 63 % of the stations and a decrease in the remaining 37 %.

Possible alternatives to this approach include nonstationary models in which changes of the distribution parameters are modeled using covariates, which are expected to be related to extreme precipitation, such as temperature (Tramblay et al., 2012; Nasri et al., 2016; Tramblay and Somot, 2018; Chagnaud et al., 2021). For the case of central and eastern Africa, Afuecheta and Omar (2021) tested a number of nonstationary models for annual and monthly maxima of daily precipitation using time as covariate, and combined them with an analysis of trends in temperature extremes with the objective of improving crop resilience and flood risk management. These methods, however, require approximations in order to reduce uncertainties. Typically, a-priori assumptions on the high-order statistical moments of the distribution (which are difficult to estimate under stationary conditions, let alone nonstationary) are used, such as the absence of temporal changes in some of the parameters (e.g., Prosdocimi and Kjeldsen, 2021). Evidence of different responses for extremes characterized by different severity (Schär et al., 2016; Pendergrass, 2018), however, challenges these assumptions. It has also been argued that stochastic climate variability may set a lower boundary to the uncertainty in the observed extremes, limiting the practical usefulness of these models (Serinaldi and Kilsby, 2015; Fatichi et al., 2016).

As an additional complication, changes in extremes may depend on the spatial scale of interest. This may alter the areal reduction factors that are used to convert in-situ estimates of extreme return levels to areal amounts associated to corresponding exceedance probabilities. These factors are of crucial importance for engineers and risk managers (Svensson and Jones, 2010). Evidence of a possible dependence on the spatial scale of the response of extremes to temperature is reported for many regions (Wasko et al., 2016; Lochbihler et al., 2017; Peleg et al., 2018), raising the question whether this effect may have caused temporal changes in the extremes in Africa.

Here, we address these challenges and try to improve our understanding of the changes that occurred in multi-scale extreme return levels in Africa over the last decades. To do so, we combine long-term high-resolution satellite precipitation estimates with a novel statistical approach able to quantify changes in return levels relevant for engineering and risk management and to attribute the observed trends to changes in the events intensity and/or occurrence. While a similar framework was recently used to investigate extreme sub-daily precipitation in the eastern Italian Alps assuming spatial homogeneity of the trends (Dallan et al., 2022), to the authors' knowledge, this is the first time this approach is applied over a wide area (here, continental) using distributed (here, satellite) information. Our application could overcome important limitations in the current state of the art for what concerns the attribution of observed trends in extremes to specific changes in precipitation climatology over wide ungauged regions of the Earth.

Specifically, we: (a) quantify trends in extreme daily precipitation amounts and extreme return levels at the local and mesoscale; (b) investigate the mechanisms underlying the observed changes; and (c) quantify differences in the changes detected for annual maximum daily amounts and extreme return levels at different spatial scales.

2. Methods

2.1. Precipitation data

This study is based on data from the Climate Hazards Group InfraRed Precipitation with Station (CHIRPS) version 2 (Funk et al., 2015), which covers the period 1981–2019 (39 years) with global land-only daily precipitation estimates at 0.05° resolution. This dataset is chosen as it represents one of the few options currently available to represent extreme daily precipitation at local and coarser scales for (i) a region where convection dominates extremes and for (ii) a sufficiently long time period to allow the investigation of temporal changes. In fact, other candidate satellite-based precipitation products generally start about two decades later, when passive microwave sensors were first deployed, and are subject to important temporal inhomogeneities in both number and type of sensors included in the estimation. Reanalysis products could represent an alternative but cannot resolve convective processes due to the insufficient resolution of the current models, and recent studies recommend the use of alternative sources when it comes to extremes: *"while we recommend caution for all products dependent on their intended application, this particularly applies to reanalyses which show the most divergence across results"* (Alexander et al. 2020).

The CHIRPS algorithm is based on infrared (IR) cold cloud duration-based precipitation estimates from the geostationary satellite constellation, and a rain gauge merging procedure. The high resolutions granted by IR are critical for sampling short-living local and mesoscale convective systems, which are crucial in determining extremes even at the daily scale (Laing et al., 2008, 2011; Raghavendra et al., 2018), especially in arid regions (Morin et al., 2020). CHIRPS is regarded as a reference in terms of robustness and quality over Africa, and is largely used in climatological studies (e.g., Dinku et al., 2018; Satgé et al., 2020; Dembélé et al., 2020). It is characterized by sufficiently high resolution and long continuous and homogeneous records to allow multi-scale trend detection over a multi-decadal period. Although Harrison et al. (2019) pointed out that *"a promising result for identifying regional changes is that numerous satellite products do well at interannual variations in precipitation totals and number of rain days, even as well as some gauge-only products"*, we limit here the possible impact of biases in the data by examining normalized quantities, namely (i) the average change rates (that is, the slope of a linear approximation of the trends normalized over the median value of the variable of interest), and (ii) the ratios between change rates. Similar assumptions have long been adopted for analyzing the scale dependence of extremes in remote sensing observations (after Frederick et al., 1977).

The Global Precipitation Climatology Center (GPCC) Full Data daily (v2020) is a 1° gridded dataset based on rain gauge observations (Ziese et al., 2020); being based on direct observations, as opposed to the indirect retrievals of the IR estimates, it is expected to provide more accurate representations of extremes, albeit at coarser spatial scales. It covers the period 1982–2019 and is used here as a benchmark for the validation of the assumptions underlying our statistical model (Section 2.4).

2.2. Statistical model

We estimate extreme return levels using a non-asymptotic statistical approach. The model relies on information from the so-called ordinary (as opposed to extreme) events, which are all the days with non-null precipitation amounts (wet days), assumed here as statistically independent (Marani and Ignaccolo, 2015; Zorzetto et al., 2016). The idea is that when the tail of the distribution of the wet-day amounts is known, an extreme value distribution describing the emerging extremes can be built from ordinary statistics, by explicitly considering the yearly sampling of wet days (Marani and Ignaccolo, 2015; Marra et al., 2020; Serinaldi et al., 2020). The approach directly captures and separates information on the wet-day intensity distribution and on wet-day occurrence frequency.

Thermodynamics reasoning suggests that the exceedance probability of extreme daily precipitation amounts x decreases as a stretched-exponential (Wilson and Toumi, 2005), so that the right tail of the wet-day distribution can be parametrized with a cumulative distribution function in the form:

$$F(x;\lambda,\kappa) = 1 - e^{-\left(\frac{x}{\lambda}\right)^{\kappa}} \tag{1}$$

where λ is a scale parameter, and κ a shape parameter which defines the tail heaviness (sub-exponential for $\kappa > 1$, heavier-than-exponential for $\kappa < 1$; see Figure S1 in the Supporting Information for a visual interpretation). This tail model was supported by observations over different climatic regimes (e.g., Papalexiou et al., 2018; Marra et al., 2019, 2020; Miniussi and Marra, 2021), including tropical Africa (Amponsah et al., 2022). Thresholds to define the tail typically ranged between the 75th and the 90th wet-day percentiles (Mediterranean and continental climates, respectively).

Knowing F, it is possible to estimate rare daily precipitation associated to extreme yearly non-exceedance probabilities p, such as the 100-year return levels with $p = 0.99$, by inverting the extreme value distribution:

$$p(x) \simeq [F(x;\lambda,\kappa)]^{n} \tag{2}$$

where the average number of wet days in a year n is explicitly considered. This approach is known as Simplified Metastatistical Extreme Value, or SMEV (Marra et al., 2019; Marra et al., 2020; Serinaldi et al., 2020).

As the model parameters are derived from a relatively large fraction of the wet-day amounts, they can be estimated for every year in the record, thus allowing us to quantify return levels at each year. These estimates will be obviously subject to large uncertainties, and will not be directly useful for engineering and risk management applications. However, using trend detection techniques, it is possible to evaluate the statistical significance of the changes in these quantities and quantify trend rates (e.g., Miniussi and Marani, 2020; Dallan et al., 2022).

2.3. Parameter estimation

In our application, we define as *wet* all daily amounts equal or exceeding 0.1 mm at 0.05° resolution, and assume independence of the wet day amounts (e.g., Zorzetto et al., 2016; Marra et al., 2019). Parameters of the model are computed for every year j: n_j is the number of wet days; λ_j and κ_j are computed by censoring (censoring the magnitude but retaining the weight in probability) the portion of data not belonging to the tail (Section 2.4), and using a least-square linear regression in Weibull-transformed coordinates (Marani and Ignaccolo, 2015).

2.4. Validation of the model assumptions and definition of the tail

Our statistical model is as good as its underlying assumption: the exceedance probability of heavy daily precipitation intensities decays as a stretched-exponential. This assumption is verified using a specific Monte Carlo test (Fig. 1), based on the one described in Marra et al. (2020). To have a quantitatively robust reference for extremes, we use the GPCC dataset. The test consists of: (i) estimating the model parameters $(\lambda^{\theta}, \kappa^{\theta})$ by explicitly censoring all the observed annual maxima and the wet-day values below a given left-censoring threshold θ; (ii) sampling 10^3 random realizations of reality as if the model assumptions were true (n_j wet days distributed as the estimated model $(\lambda^{\theta}, \kappa^{\theta})$ with $j = 1, \cdots, M$ representing years in the record); (iii) extracting the corresponding annual maxima; (iv) testing whether the observed annual maxima are likely samples from the model: if more than 5% of these annual maxima lie outside the 95% sampling confidence interval, the assumption of having stretched-exponential tail above the tested threshold is to be rejected. Iterating (i)-(iv) over different thresholds θ permits to identify the portion of the distribution tail which is well described by a stretched-exponential, that is the lowest threshold above which the model is never rejected. Left-censoring thresholds between the 50th and the 90th percentile are explored. If the stretched-exponential tail is rejected also for the highest left-censoring threshold, we consider the assumption as not verified. Because the tail is expected to be a climatic property and the test is subject to a level of stochasticity, the left-censoring thresholds used in the study are selected by smoothing the obtained values (1° resolution) over 3° × 3° windows and rounding to the closest 5th percentile. A schematic of the workflow is reported in Fig. 1.

It is worth noting three aspects concerning this test. First, for the sake of the test, the stationarity assumption behind the test (a unique tail is tested using all the years) can be considered verified, even when significant trends are observed (Figure S2). Second, the test is robust: the probability of not rejecting stretched-exponential tails in presence of power-type tails, which are the most widely supported alternative to stretched-exponential tails for the case of precipitation, is zero or close to zero for thresholds lower than the 90th percentile; conversely, the probability of wrong rejection in presence of stretched-exponential tails can be close to 10% (Figure S3). Last, our definition of the left-censoring thresholds implies that the model parameters are not sensitive to small changes in the thresholds (see Marra et al., 2019).

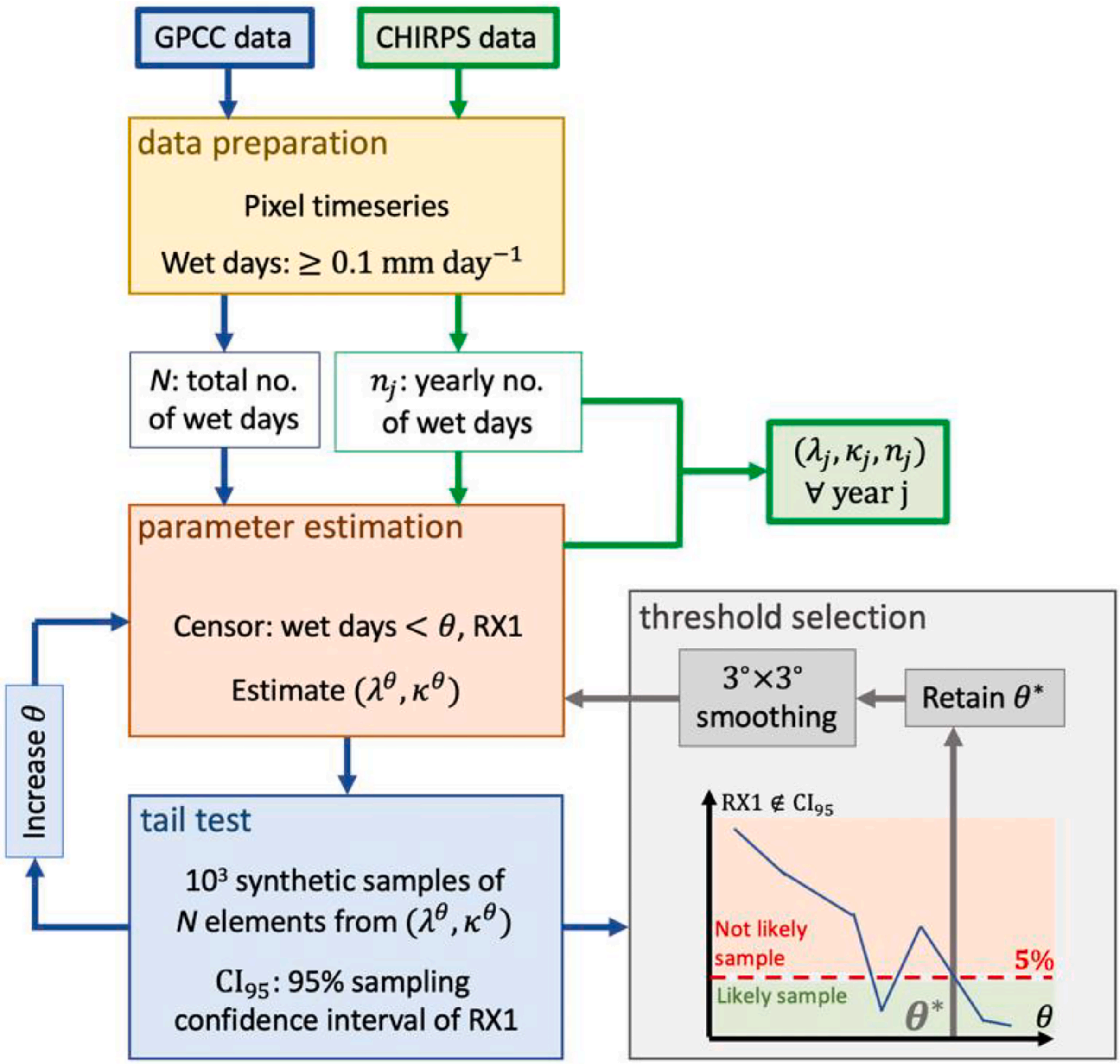

Fig. 1. Workflow of the test to verify the tail assumption and define the tail.

2.5. *Spatial scales*

Two spatial scales are examined: (i) *local* scale, represented by CHIRPS data at the original resolution (0.05°, ~5 km at the equator); (ii) *meso*scale, represented by the data aggregated to 1° resolution (~100 km at the equator). To do so, a 1°-aggregated value is computed for each wet day of the 0.05° pixels by spatially averaging the original data over the 20 × 20 surrounding pixels.

2.6. *Detection of temporal trends*

The non-parametric Mann-Kendall test (Mann, 1945) is used to test the statistical significance (level $\alpha = 0.05$) of the trends in the model parameters, in the largest daily amounts observed (RX1) and modeled (RX1 modelled) in each year, and in the modeled return levels (100-year return levels are here shown), at both local and mesoscale. The 2-year return levels are the theoretical median of RX1 and are here used as model quantification of the change rate in the RX1 (RX1 modeled). Possible serial correlation in the data is accounted for by pre-whitening the data; it should be noted that correlation was small, and results without pre-whitening are indistinguishable. Yearly estimates of the distribution parameters may be subject to systematic biases, especially for what concerns the estimated tail heaviness (usually, tail heaviness is overestimated when few data are available for parameter estimation). To limit the impact of this issue, the magnitude of the trends is here quantified using the average change rate, computed as the ratio between the non-parametric Sen's slope estimator (Sen, 1968) and the median value of the variable in the time series. This assumes that the biases in the estimated parameters are stationary.

3. Results and discussion

3.1. *Tail properties of extreme daily precipitation over Africa*

The right tail of the distribution of daily precipitation amounts is found to be well described by a stretched-exponential model for ~87% of the continent (see Fig. 2), with definitions of the right tail ranging from the largest 50% of the wet day amounts (light blue in the Fig. 2a) to the largest 10% (dark blue). In the remaining ~13% of the continent (dotted areas), our test rejects the assumption of stretched-exponential tail within the tested ranges of tail definitions (50th to 90th percentiles). As mentioned above, this is in-line with synthetic experiments

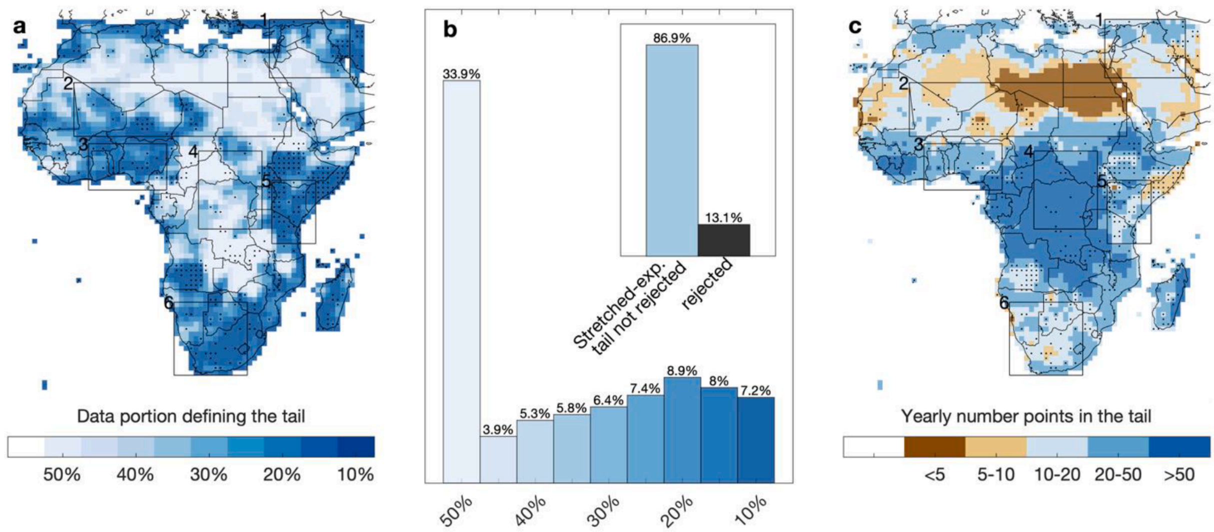

Fig. 2. Tail properties of extreme precipitation in Africa. (a) Portion of wet-day amounts defining the stretched-exponential tail as identified using the test on the GPCC data (after the $3^\circ \times 3^\circ$ smoothing); light blue shades represent areas in which the largest 50% (or more) of the data follow a stretched-exponential model, dark blue shades areas in which the largest 10% of the data follow a stretched-exponential model. Dotted pixels represent areas in which the test could not identify a stretched-exponential tail. (b) Fraction of pixels for which the stretched-exponential tail assumption is verified (inset) and, for the verified ones, fraction on pixels belonging to each tail definition. (c) Average yearly number of wet-days in the tail as defined using the proportions in (a).

showing that, under the examined conditions (record length, yearly number of wet days), the test may provide ~5–11% false rejections (see Figure S3). However, in two regions (one in east Africa and one in southern Angola) the spatial clustering of these pixels suggests that extreme precipitation could have different types of tail or that tails could here consist in smaller fractions of the data (e.g., only the largest 5%). Nevertheless, since only few significant trends are detected in these areas (see next section), this is not expected to affect our results. After left-censoring, an average of at least 10 data points per year are available for parameter estimation in most of the continent (Fig. 2c), granting a proper estimation of the two tail parameters; fewer data points are available over the Sahara Desert and in other isolated areas in the eastern and southern portions of the continent.

3.2. *Trends in annual maximum daily precipitation*

The trends of the annual maximum daily precipitation (RX1) at the local scale are significant over 20.3% of the continent (Fig. 3a). The area in central Africa characterized by strong negative trends (area #4 in Fig. 3a) contributes ~60% of the significant trends; however, the reliability of the results is dubious because the area is almost completely devoid of ground observations. In particular, central Africa is a region where rain gauge data are scarce with consequences on the accuracy of the satellite precipitation products, which strongly rely on gauge data for their generation, as is the case of CHIRPS. The case of the central Africa will be further discussed below (Section 3.2.1).

Without considering the central African area, ~37% of the significant trends is positive and ~63% negative. Positive trends are reported in the Sahel (#2), in Kenya and Tanzania (#5), and in the coastal regions of the Gulf of Guinea (#3) and of the Middle East (#1); negative trends are reported in the Middle East (#1), in inland areas of west Africa (#3 and #2), in South Africa and Namibia (#6), and in the above mentioned region in central Africa extending from Sudan to Angola (#4). Similar trends are reported at the mesoscale (1°; Figure S4). The fraction of significant trends in the six examined areas ranges from 15% to 20.1%, and reaches ~77% in area #4 (13.4–74% at the mesoscale), and are thus larger than the 5% false positives expected at the used significance level. The interested reader can find quantitative information on the parameters estimated for the different areas in Table S1. These values are reasonable when compared to other studies in which stretched-exponential tails have been used (e.g., Marra et al., 2020; Miniussi and Marra, 2021); nevertheless, as discussed in Section 2.6, we deem their quantitative values less reliable than the average change rates examined here.

Harrison et al. (2019) compared trends derived from multiple precipitation products, including CHIRPS, finding no statistically significant change in the extremes. Direct comparison with their results is however difficult, because they focused on a small portion of the continent in which our results show no statistically significant trend (see Fig. 1 in Harrison et al., 2019). Similarly, Pfahl et al. (2017) reported an increase in RX1 from global climate models in central Africa for the period 1983–2000, a result difficult to compare with ours due to the different examined period and to the known deficiency of global models in resolving the convective processes that are key to extreme precipitation. The trends we observe, however, are in line with results from both Chaney et al. (2014), who reported positive trends in the Sahel region, and Mtewele et al. (2021), who used multi-sensor satellite estimates from the Tropical Rainfall Measurement Mission (TRMM) Multi-satellite Precipitation Analysis (TMPA) for the period 1998–2018 and found negative trends in both frequency and intensity of extremes in the western portion of central Africa.

3.2.1. *The case of the central Africa*

The area over which consistent negative trends in extremes are observed includes the tropical forests of the Congo basin and vast savannah regions (D'Onofrio et al., 2018). Since most of the precipitable water available in these regions is related to the forest or to other vegetation types (O'Connor et al., 2021), vegetation-precipitation feedbacks may represent an important mechanism behind these observations (e.g., due to wildfire-generated aerosols or woody encroachment), a hypothesis to be explored more in detail in the future.

Other authors recently highlighted a decrease in precipitation amounts and forest greenness over Congo, with an increase of the dry season length (Jiang et al., 2019; Zhou et al., 2014). Convection (from deep convection to mesoscale convective systems) is responsible for most of precipitation in this area, being the Congo Basin one of the three most convective regions in the world together with Amazonia and the Indonesian maritime continent. Raghavendra et al. (2018) used 35 years (1982–2016) of geostationary infrared brightness temperatures to explore the changes in the magnitude and area of cold cloud top

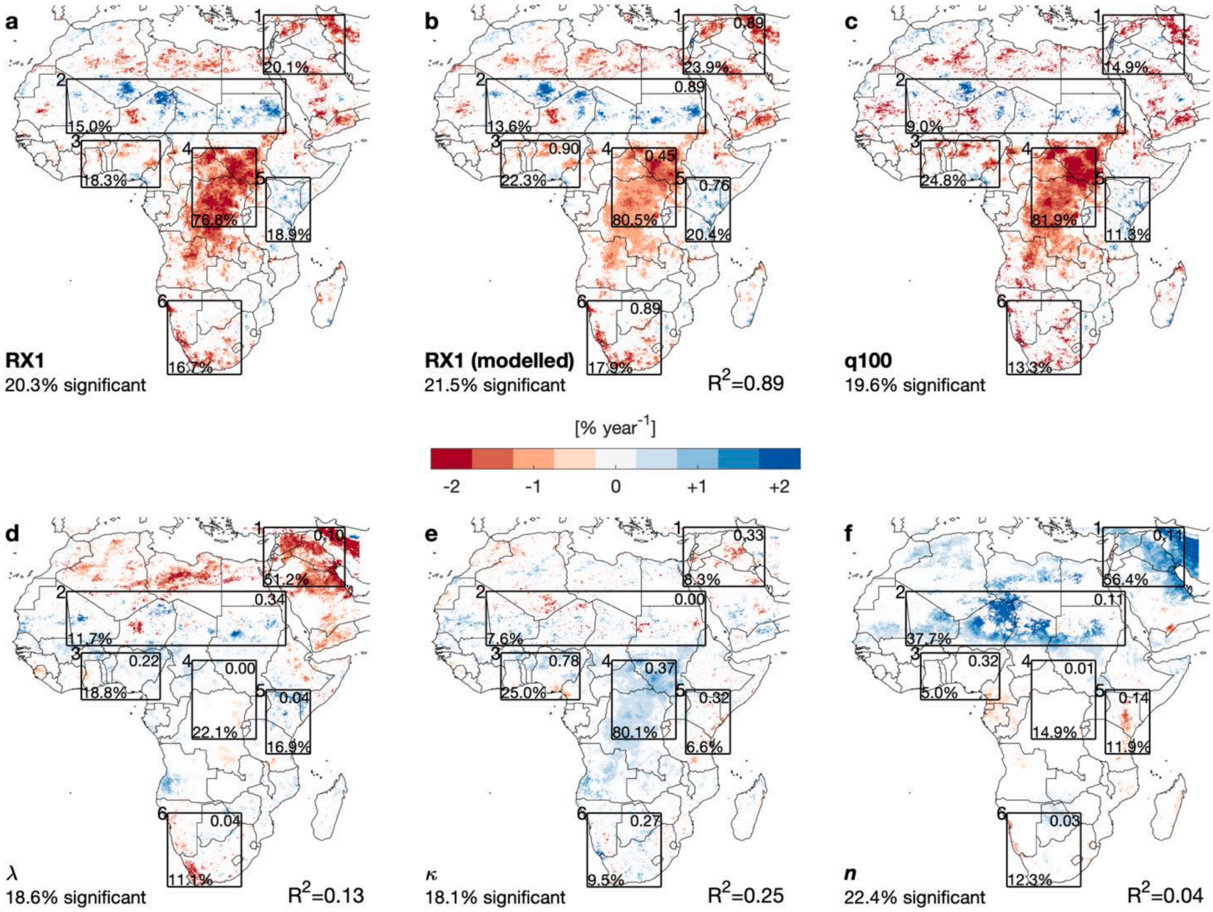

Fig. 3. Observed and modelled trends at the local scale (0.05°). The average change rate of significant (Mann-Kendall test, $\alpha = 0.05$) trends is shown. (a) Trends in the observed annual maximum daily precipitation (RX1); the fraction of pixels with significant trend is reported for the whole study area (bottom left) and for each area (bottom left in each box); (b) Modelled trends in RX1; R^2 with the trends in observed RX1 is reported for the whole study area (bottom right) and for each area (top right in each box); the model explains 89% of the variance in the trends of observed RX1; (c) Modelled trends in the 100-year daily precipitation (q100); (d) trends in the scale parameter of the model (λ); changes in the scale explain 13% (0–34% depending on the region) of the variance in the trends of observed RX1; (e) Trends in the shape parameter of the model (κ); changes in tail heaviness explain 25% (0–78% depending on the region) of the variance in the trends of observed RX1; (f) Trends in the average yearly number of wet days (n); changes in the number of wet days explain 4% (1–32% depending on the region) of the variance in the trends of observed RX1. Observed and modelled trends at the mesoscale (1°) are reported in Figure S4.

temperatures as a proxy for the number and size of individual thunderstorms at different intensities. The results suggest that larger and more intense thunderstorms are occurring in this area during the last decades, with an increase in the mean size of thunderstorms with lower cloud top temperature to the detriment of the mean size of thunderstorms with higher cloud top temperature. This contributes to a drier lower troposphere (and a wetter higher troposphere), a weaker ascent at both the lower and upper troposphere, and an overall reduction of the soil moisture. These changes were found to be associated with a significant decrease in April-May-June precipitation over the Congo Basin. More recently, Alber et al. (2021) analyzed the trend in thunderstorm activity from 1983 to 2018 exploiting the Gálvez-Davidson index. Feedback mechanisms are proposed to explain the observed thunderstorm intensification, which include the cooling and moistening of the mid-troposphere, drying and warming at the surface and lower troposphere, and a decrease in vertical stability and convective inhibition. Despite the lower level of accuracy expected for CHIRPS estimates in this region, the above factors are conducive to the significant negative trend we observe for the past 40 years, which is also in agreement with rather independent satellite observations for the last ~20 years (Mtewele et al., 2021).

3.3. Evaluation of the statistical model

Our statistical model proves robust at reproducing the observed trends both in qualitative (spatial patterns) and quantitative (explained variance) terms (Fig. 3b). Specifically, the model explains 89% of the variance (91% at the mesoscale) of the significant change rates (R^2 computed for all pixels in which the observed trend is significant). Notably, only 45% of the variance (43% at the mesoscale) is explained in area #4, while 76–90% of the variance (68–92% at the mesoscale) is explained in the other areas. Remarkably, the model run explicitly censoring the observed annual maxima (RX1), and thus providing independent estimates of their trends, explains as much as 72% of the variance (67% at the mesoscale) of the significant trends in RX1 (Fig. 4). This suggests that the proposed statistical model could represent an opportunity for examining trends in extremes in situations in which the observed/modelled extremes are not fully trusted (e.g., Masunaga et al., 2019; Rajulapati et al., 2020). These results support the use of the statistical model to (i) investigate the relation between daily precipitation climatology and extreme and (ii) quantify trends in rare exceedance probabilities which cannot be extracted from observations alone, as detailed in the following sections.

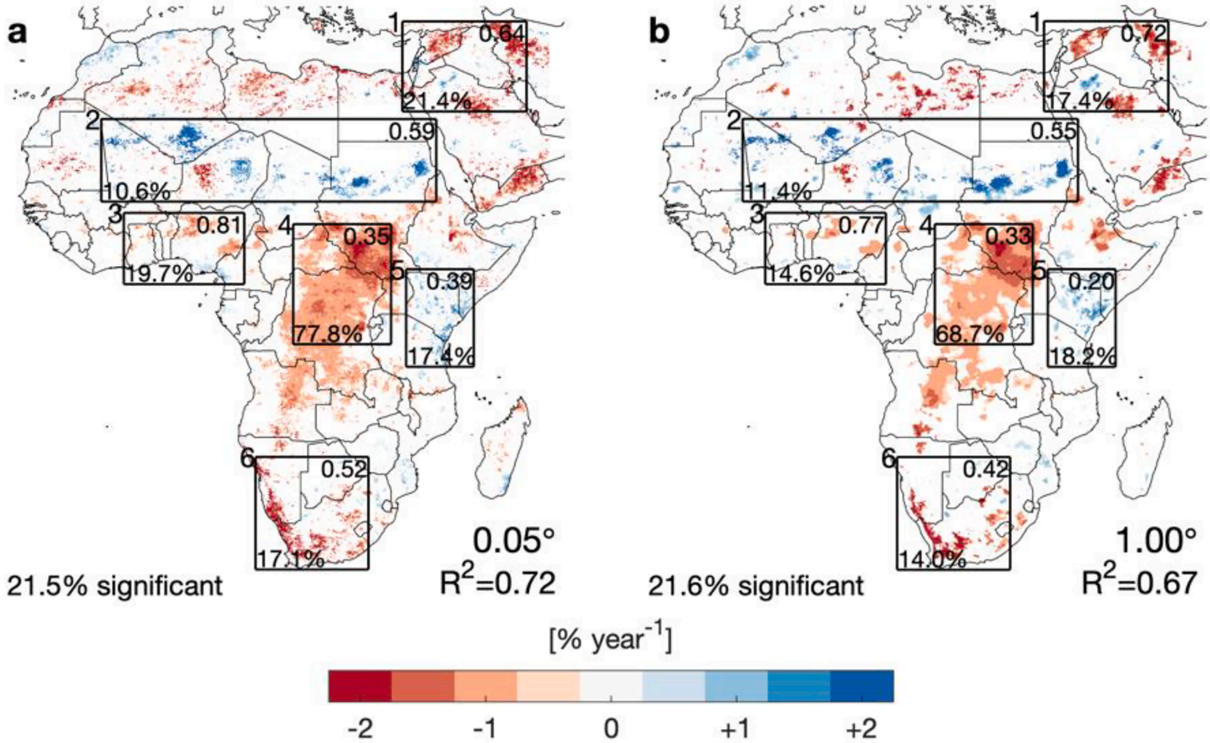

Fig. 4. Empirical validation of the model assumptions: trends in RX1 modelled explicitly censoring the observed RX1. Average change rate of significant (Mann-Kendall test, $p_{value} < 0.05$) trends in RX1 modelled by explicitly censoring the observed annual maxima at local (a) and mesoscales (b). The fraction of pixels with significant trend is reported for the whole study area (bottom left) and for each area (bottom left in each box); R^2 with the trends in observed RX1 is reported for the whole study area (bottom right) and for each area (top right in each box). The censored model reproduces 72% of the variance (67% at the mesoscale) in the significant trends of the observed RX1.

3.4. Link between changes in precipitation climatology and extremes

The largest portion of variance explained by the model is to be ascribed to the distribution tail heaviness (shape parameter of the stretched exponential distribution κ, which is negatively correlated to extreme return levels; see Figure S1) with 25% explained variance (38% at the mesoscale; Fig. 3e and Figure S4e). Changes in the scale of the distribution λ explain 13 % of the variance (21% at the mesoscale), and changes in the number of wet days 4% (12% at the mesoscale) (Fig. 3d and f; Figure S4d and S4f). This implies that, at both scales, the trends in extremes are mostly related to changes in the distribution of daily precipitation amounts, rather than to changes in the occurrence frequency of storms and, mostly, in the proportion of very extreme events. An interesting exception is the Sahel (area #2), where the number of wet days explains 11% of the variance versus 0% of the tail heaviness. This confirms previous findings based on in-situ and satellite observations (Panthou et al., 2014; Taylor et al., 2017; Chagnaud et al., 2021). Possible physical explanations are associated with changes in sea surface temperature, convective available potential energy, and vertical wind shear, and are discussed by Biasutti (2019), and Tramblay et al. (2020). Noting that a uniform scaling of extreme precipitation with temperature (such as 7% $°C^{-1}$ expected according to the Clausius-Clapeyron relation; e.g., O'Gorman and Schneider, 2009) translates into a change in the scale parameter only, the trends we observe in the model parameter imply that severity-dependent scaling factors are essential to adequately capture the complex dependences of extreme precipitation, and that trends in extreme return levels are likely different from the trends one can detect using observed annual maxima.

3.5. Different changes of annual maxima and extreme return levels at local and mesoscales

Significant trends in the 100-year return levels (q100) derived from the statistical model are shown in Fig. 3c (Figure S4c for the mesoscale). Overall, 19.6% of the continent experienced significant changes in the 100-year events. This implies that the stochastic uncertainties characterizing yearly estimates of extreme return levels as high as the 100-year events using our model is comparable to the one characterizing annual maxima. The spatial patterns of these changes largely follow the ones of RX1, with no cases of opposing trends, but their magnitude is always (99.99% of the significant pixels) greater (Fig. 5). Trend rates in the 100-year events in Africa since 1981 have been ~44% stronger (in median) than the ones in RX1, both at local and mesoscales. This is consistent with previous findings based on extreme precipitation-temperature scaling, observations, and models in several regions of the Earth (e.g., Myhre et al., 2019; Kelder et al., 2020; Lenderink et al., 2021; Visser et al., 2021).

The ratio between change rates of extremes at local and mesoscales can be interpreted as a proxy of the changes in extreme storm structure, and is directly related to the areal reduction factors (Fig. 6). The previously reported redistribution of moisture toward the storm center in response to global warming (e.g., Wasko et al., 2016; Armon et al., 2022) translates into expected stronger positive trends at the local scale, or stronger negative trends at the mesoscale. This is qualitatively confirmed in areas #3 (positive trends) and #6 (negative), and implies an increased reduction of extremes with area in some parts of eastern Africa and southern Africa (Fig. 6b and d). However, other regions present opposite behaviors, such as area #1 (both positive and negative trends), area #2 (positive) and area #4 (negative). This smoothing translates into a decreased reduction of extremes with area, and confirms previous findings based on the Sahel (Vischel et al., 2019). Overall,

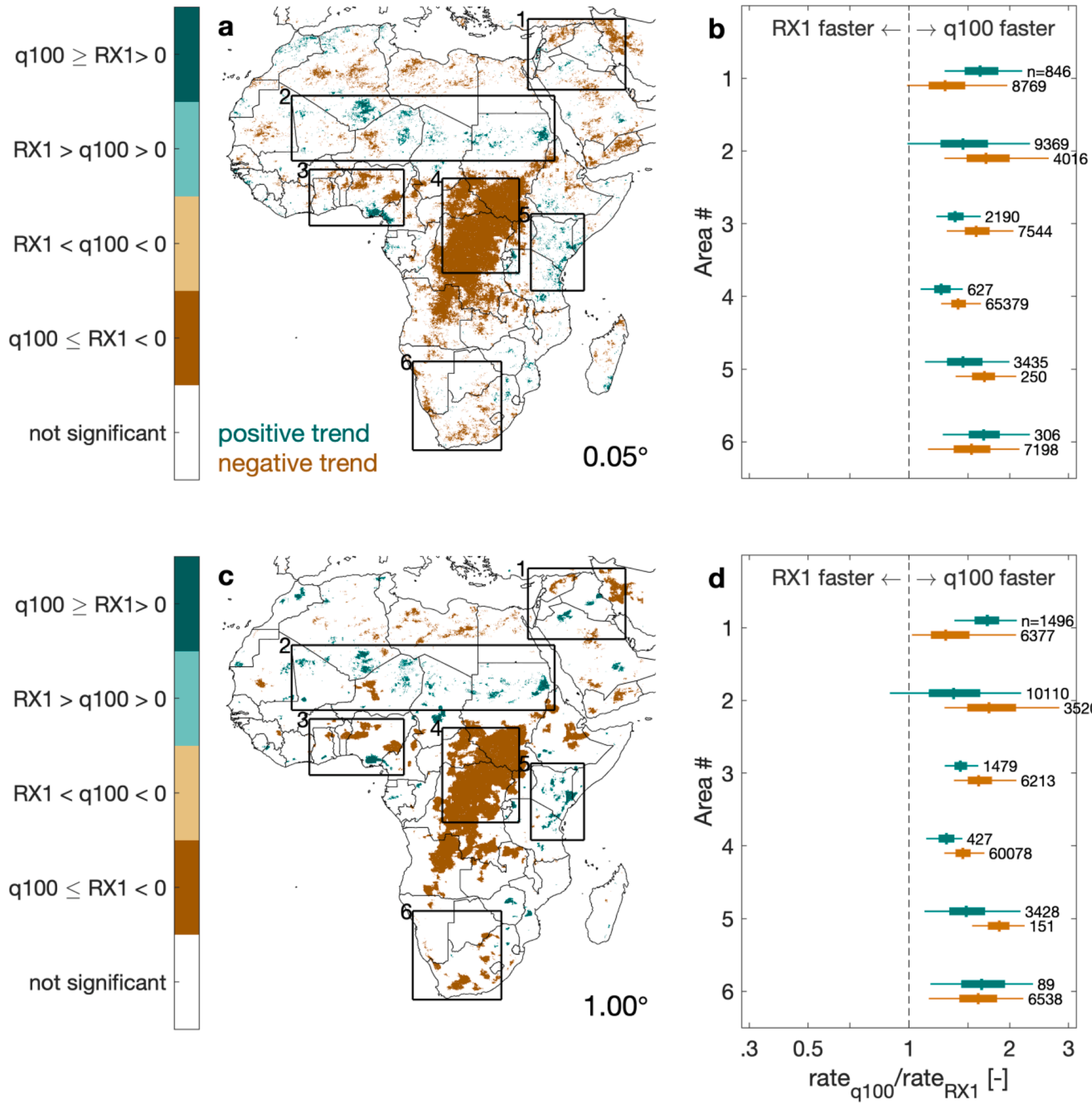

Fig. 5. Extreme daily precipitation return levels changed faster than annual maxima. (a) Relative magnitude of increasing (blue shades) and decreasing (brown shades) trends between extreme return levels (here 100-year events are shown, q100) and annual maximum daily precipitation (RX1) at the local scale (0.05°); (b) Ratio between the average change rate of q100 and RX1 in the six areas at the local scale (median, inter-quartile range and 5-95th percentile range are shown); the number of considered pixels (both trends are significant) is reported next to each boxplot; (c) Relative magnitude of increasing and decreasing trends between q100 and RX1 at the mesoscale (1°); (d) Ratio between the average change rate of q100 and RX1 in the six areas at the mesoscale; the number of considered pixels (both trends are significant) is reported next to each boxplot. In all panels, only pixels in which both trends are significant (Mann-Kendall test, $\alpha = 0.05$) and concordant (discordant trends are found in ≤ 7 pixel) are shown.

the distribution of these ratios is rather dispersed, so that local situations might largely differ from the behaviors highlighted here; specific cases need to be examined individually.

When interpreting our results in terms of risk assessment and water resources management, we should consider systems that respond to daily or sub-daily extreme rainfall, such as floods and flash-floods in catchments with areas up to a few thousand square kilometers, or landslides and debris flows in headwater catchments and steep slopes. The faster changes in extreme return levels, here demonstrated by the 100-year events, imply that changes in the potential occurrence of these hazards could have happened faster than what measured by usual trends on RX1. The strong positive trends observed in Area #2 (Sahel) and #5 (eastern Africa), for example, could be indicative of a quick increase in the probability of flood and landslides in these areas over the past decades, as perhaps exemplified by recent events (Wainwright et al., 2021). Similarly, the change we report in the areal reduction factors can suggest different changes between landslides/flash-flood risk, which respond to local precipitation, and flood risk/water availability, which are mostly impacted by the volumes of precipitation over relatively vast areas. However, it should be recalled that rainfall is far from being the only factor affecting these processes (e.g., Sharma et al., 2018). Additional work based on hydrological models or slope stability models able to include observed trends in extremes, antecedent conditions, and other relevant processes is needed to thoroughly address these issues quantitatively.

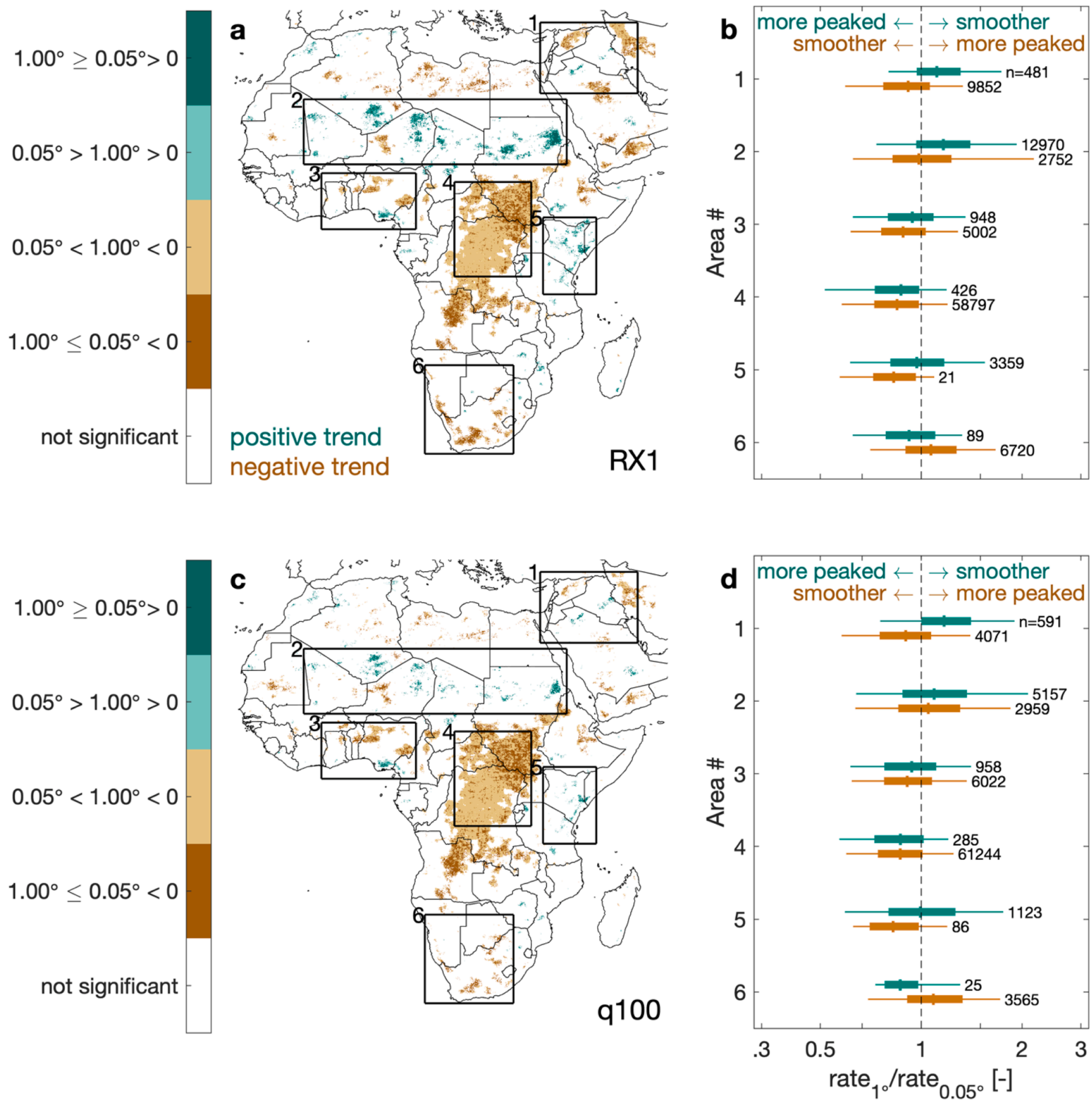

Fig. 6. Different changes in extreme precipitation at the local and mesoscale. (a) Relative magnitude of the increasing (blue shades) and decreasing (brown shades) trends between local (0.05°) and mesoscale (1°) for the annual maximum daily precipitation (RX1); (b) Ratio between the average change rate of RX1 at local and mesoscale in the six areas (median, inter-quartile range and 5-95th percentile range are shown); the number of considered pixels (both trends are significant) is reported next to each boxplot; (c) Relative magnitude of the increasing and decreasing trends between local and mesoscale for extreme return levels (here 100-year events are shown, q100); (d) Ratio between the average change rate of q100 at local and mesoscale in the six areas; the number of considered pixels (both trends are significant) is reported next to each boxplot. In all panels, only pixels in which both trends are significant (Mann-Kendall test, $\alpha = 0.05$) are shown (all trends are concordant).

4. Conclusions

Changes in annual maximum daily precipitation and low-probability extremes relevant for engineering and risk management that occurred over Africa since 1981 are examined using a high-resolution satellite precipitation product (CHIRPS Version 2) and a novel non-asymptotic statistical approach based on ordinary (as opposed to extreme-value) statistics. Temporal trends in annual maxima (RX1) and extreme return levels at local scales (0.05°) and mesoscales (1°) are detected, quantified, and compared, and are then attributed to changes in wet-day occurrence and characteristics of the wet-day intensity distribution.

Roughly 20% of the continent experienced significant trends (Mann-Kendall, $\alpha = 0.05$) in annual maxima (RX1), with both positive (Sahel, Kenya and Tanzania, coastal regions of the Gulf of Guinea, coastal regions of the Middle East) and negative (Middle East, inland areas of west Africa, South Africa and Namibia, and a vast region in central Africa extending from Sudan to Angola) changes.

The statistical model explains 89% (91% at the mesoscale) of the variance in the observed change rates of RX1, and 72% (67% at the mesoscale) of the variance when run with explicit censoring of the observed annual maxima. It can thus be trusted for investigating causal relations between wet-day intensity distribution and number of wet days, on one side, and extremes on the other, and to quantify past trends in rare exceedance probabilities. Provided its assumptions are met, it could represent a viable option for examining trends in situations in which the observed/modelled extremes are not fully trusted. Here, we evaluated the validity of the model assumption using observational data and a robust Monte Carlo-based statistical test.

Changes in the tail heaviness of the wet-day intensity distribution, that is the proportion between heavy and extreme events, explain most (25%) of the variance in the changes in RX1, as opposed to 13% of the intensity distribution scale parameter and 4% of the number of wet days. These results imply a differential rate of change between RX1 and rarer extremes: extreme return levels changed faster than RX1 (∼44% faster for the case of 100-year events), both for positive and negative trends. Increased reduction of extremes with area, suggesting a redistribution of moisture toward the storm center, is reported for coastal areas of the Gulf of Guinea (positive trends) and southern Africa (negative), while an opposite behavior is found for the Middle East (positive and negative trends), Sahel (positive), and central Africa (negative). These results imply locally-dependent impacts on the areal reduction factors used to derive extreme return levels at the areal scale (e.g., at the catchment scale).

Our quantitative results depend on the ability of CHIRPSv2 to represent changes in the wet-day precipitation intensities and in precipitation occurrence, key features of our model, and on the local adequacy of the stretched-exponential tail model and of the assumptions underlying the trend analyses, but are robust with respect to stochastic uncertainties and errors in the satellite estimation of extreme precipitation.

CRediT authorship contribution statement

Francesco Marra: Conceptualization, Formal analysis, Writing – review & editing. **Vincenzo Levizzani:** Data curation, Writing – review & editing. **Elsa Cattani:** Data curation, Writing – review & editing.

Declaration of Competing Interest

The authors declare that they have no known competing financial interests or personal relationships that could have appeared to influence the work reported in this paper.

Data availability

Links to the data are provided in the acknowledgements

Acknowledgements

The study was supported by funding from internal projects of the CNR-ISAC Institute. The authors thank Eleonora Dallan for the discussions about the statistical model, Mara Baudena for the discussion about precipitation-vegetation feedbacks, and Laura Harrison for the discussion about the CHIRPS dataset. CHIRPSv2 data can be retrieved from https://data.chc.ucsb.edu/products/CHIRPS-2.0/africa_daily/tifs/p05/ [accessed Feb 10, 2021]. GPCC Full Data daily v2020 can be retrieved from https://www.dwd.de/EN/ourservices/gpcc/gpcc.html [accessed Jan 21, 2021]. Codes and elaborated data to reproduce the results of this study are available at https://doi.org/10.5281/zenodo.6257415.

Appendix A. Supplementary data

Supplementary data to this article can be found online at https://doi.org/10.1016/j.hydroa.2022.100130.

References

Afuecheta, E., Omar, M.H., 2021. Characterization of variability and trends in daily precipitation and temperature extremes in the Horn of Africa. Climate Risk Manag. 32, 100295 https://doi.org/10.1016/j.crm.2021.100295.

Aguilar, E., Barry, A.A., Brunet, M., Ekang, L., Fernandes, A., Massoukina, M., Mbah, J., Mhanda, A., do Nascimento, Peterson, T.C., Thamba Umba, O., Tomou, M., Zhang, X., 2009. Changes in temperature and precipitation extremes in western central Africa, Guinea Conakry, and Zimbabwe, 1955–2006. J. Geophys. Res. 114, D02115. https://doi.org/10.1029/2008JD011010.

Alber, K., Raghavendra, A., Zhou, L., Jiang, Y., Sussman, H.S., Solimine, S.L., 2021. Analyzing intensifying thunderstorms over the Congo Basin using the Gálvez-Davison index from 1983–2018. Clim. Dyn. 56, 949–967. https://doi.org/10.1007/s00382-020-05513-x.

Alexander, L.V., Bador, M., Roca, R., Contractor, S., Donat, M.D., Nguyen, P.L., 2020. Intercomparison of annual precipitation indices and extremes over global land areas from in situ, space-based and reanalysis products. Env. Res. Lett. 15, 055002 https://doi.org/10.1088/1748-9326/ab79e2.

Amponsah, W., Dallan, E., Nikolopoulos, E.I., Marra, F., 2022. Climatic and topographic controls on rainfall extremes and their temporal changes in data-sparse tropical regions. J. Hydrol. 612, 128090 https://doi.org/10.1016/j.jhydrol.2022.128090.

Armon, M., Marra, F., Enzel, Y., Rostkier-Edelstein, D., Garfinkel, C.I., Adam, O., Dayan, U., Morin, E., 2022. Reduced rainfall in future heavy precipitation events related to contracted rain area despite increased rain rate. Earth's Future 9. https://doi.org/10.1029/2021EF002397 e2021EF002397.

Biasutti, M., 2019. Rainfall trends in the African Sahel: Characteristics, processes, and causes. WIREs Climate Change 10, e591.

Cattani, E., Merino, A., Guijarro, J.A., Levizzani, V., 2018. East Africa rainfall trends and variability 1983–2015 using three long-term satellite products. Remote Sens. 10, 931. https://doi.org/10.3390/rs10060931.

Chagnaud, G., Panthou, G., Vischel, T., Blanchet, J., Lebel, T., 2021. A unified statistical framework for detecting trends in multi-timescale precipitation extremes: application to non-stationary intensity-duration-frequency curves. Theor. Appl. Climatol. 145, 839–860. https://doi.org/10.1007/s00704-021-03650-9.

Chaney, N.W., Sheffield, J., Villarini, G., Wood, E.F., 2014. Development of a high-resolution gridded daily meteorological dataset over Sub-Saharan Africa: Spatial analysis of trends in climate extremes. J. Climate 27, 5815–5835. https://doi.org/10.1175/JCLI-D-13-00423.1.

Coles, S., 2001. An introduction to statistical modeling of extreme values. Springer-Verlag, London.

Contractor, S., Donat, M.G., Alexander, L.V., Ziese, M., Meyer-Christoffer, A., Schneider, U., Rustemeier, E., Becker, A., Durre, I., Vose, R.S., 2020. Rainfall Estimates on a Gridded Network (REGEN) – A global land-based gridded dataset of daily precipitation from 1950 to 2016. Hydrol. Earth Syst. Sci. 24, 919–943. https://doi.org/10.5194/hess-24-919-2020.

D'Onofrio, D., von Hardenberg, J., Baudena, M., 2018. Not only trees: Grasses determine African tropical biome distributions via water limitation and fire. Global Ecol. Biogeog. 27, 714–725. https://doi.org/10.1111/geb.12735.

Dallan, E., Borga, M., Zaramella, M., Marra, F., 2022. Enhanced summer convection explains observed trends in extreme subdaily precipitation in the northeastern Italian Alps. Geophys. Res. Lett. 49 https://doi.org/10.1029/2021GL096727 e2021GL096727.

De Waal, J.H., Chapman, A., Kemp, J., 2017. Extreme 1-day rainfall distributions: Analysing change in the Western Cape. S.Afr. J. Sci. 113 (7/8) https://doi.org/10.17159/sajs.2017/20160301, 2016-0301.

Dembélé, M., Schaefli, B., van de Giesen, N., Mariéthoz, G., 2020. Suitability of 17 gridded rainfall and temperature datasets for large-scale hydrological modelling in West Africa. Hydrol. Earth Syst. Sci. 24, 5379–5406. https://doi.org/10.5194/hess-24-5379-2020.

Di Baldassarre, G., Montanari, A., Lins, H., Koutsoyiannis, D., Brandimarte, L., Blöschl, G., 2010. Flood fatalities in Africa: from diagnosis to mitigation. Geophys. Res. Lett. 37, L22402. https://doi.org/10.1029/2010GL045467.

Diatta, S., Diedhiou, C.W., Dione, D.M., Sambou, S., 2020. Spatial variation and trend of extreme precipitation in West Africa and teleconnections with remote indices. Atmosphere 11, 999. https://doi.org/10.3390/atmos11090999.

Dinku, T., Funk, C., Peterson, P., Maidment, R., Tadesse, T., Gadain, H., Ceccato, P., 2018. Validation of the CHIRPS satellite rainfall estimates over eastern Africa. Quart. J. Roy. Meteor. Soc. 144, 292–312. https://doi.org/10.1002/qj.3244.

Fatichi, S., Ivanov, V.Y., Paschalis, A., Peleg, N., Molnar, P., Rimkus, S., Kim, J., Burlando, P., Caporali, E., 2016. Uncertainty partition challenges the predictability of vital details of climate change. Earth's Future 4 (5), 240–251. https://doi.org/10.1002/2015EF000336.

Frederick, R.H., Myers, V.A., Auciello, E.P., 1977. Storm depth-area relations from digitized radar returns. Water Resour. Res. 13 (3), 675–679. https://doi.org/10.1029/WR013i003p00675.

Funk, C., Peterson, P., Landsfeld, M., Pedreros, D., Verdin, J., Shukla, S., Husak, G., Rowland, J., Harrison, L., Hoell, A., Michaelsen, J., 2015. The climate hazards infrared precipitation with stations—A new environmental record for monitoring extremes. Sci. Data 2, 150066. https://doi.org/10.1038/sdata.2015.66.

Gebrechorkos, S.H., Hülsmann, S., Bernhofer, C., 2019. Changes in temperature and precipitation extremes in Ethiopia, Kenya, and Tanzania. Int. J. Climatol 39, 18–30. https://doi.org/10.1002/joc.5777.

Harrison, L., Funk, C., Peterson, P., 2019. Identifying changing precipitation extremes in Sub-Saharan Africa with gauge and satellite products. Environ. Res. Lett. 14, 085007 https://doi.org/10.1088/1748-9326/ab2cae.

Igwe, O., 2018. The characteristics and mechanisms of the recent catastrophic landslides in Africa under IPL and WCoE projects. Landslides 15, 2509–2519. https://doi.org/10.1007/s10346-018-1064-3.

IPCC: Climate Change 2021: The Physical Science Basis. Contribution of Working Group I to the Sixth Assessment Report of the Intergovernmental Panel on Climate Change V Masson-Delmotte, P Zhai, A Pirani, S L Connors, C Péan, S Berger, N Caud, Y Chen, L Goldfarb, M I Gomis, M Huang, K Leitzell, E Lonnoy, J B R Matthews, T K Maycock, T Waterfield, O Yelekçi, R Yu, B Zhou (eds.). Cambridge University Press. In Press., 2021.

Jiang, Y., Zhou, L., Tucker, C.J., Raghavendra, A., Hua, W., Liu, Y.Y., Joiner, J., 2019. Widespread increase of boreal summer dry season length over the Congo rainforest. Nat. Clim. Chang. 9, 617–622. https://doi.org/10.1038/s41558-019-0512-y.
Katz, R.W., Parlange, M.B., Naveau, P., 2002. Statistics of extremes in hydrology. Adv. Water Resour. 25 (8–12), 1287–1304. https://doi.org/10.1016/S0309-1708(02)00056-8.
Kelder, T., Müller, M., Slater, L.J., Marjoribanks, T.I., Wilby, R.L., Prudhomme, C., Bohlinger, P., Ferranti, L., Nipen, T., 2020. Using UNSEEN trends to detect decadal changes in 100-year precipitation extremes. Npj Climate Atmos. Sci. 3, 47. https://doi.org/10.1038/s41612-020-00149-4.
Kidd, C., Becker, A., Huffman, G.J., Muller, C.L., Joe, P., Skofronick-Jackson, G., Kirschbaum, D., 2017. So, how much of the Earth's surface is covered by rain gauges? Bull. Amer. Meteor. Soc. 98 (1), 69–78. https://doi.org/10.1175/BAMS-D-14-00283.
Kruger, A.C., Nxumalo, M.P., 2017. Historical rainfall trends in South Africa: 1921–2015. Water SA 43 (2), 285–297. https://doi.org/10.4314/wsa.v43i2.12.
Laing, A.G., Carbone, R.E., Levizzani, V., Tuttle, J., 2008. The propagation and diurnal cycles of deep convection in northern tropical Africa. Quart. J. Roy. Meteor. Soc. 134, 93–109. https://doi.org/10.1002/qj.194.
Laing, A.G., Carbone, R.E., Levizzani, V., 2011. Cycles and propagation of deep convection over equatorial Africa. Mon. Wea. Rev. 139, 2832–2853. https://doi.org/10.1175/2011MWR3500.1.
Lenderink, G., de Vries, H., Fowler, H.J., Barbero, R., van Ulft, B., van Meijgaard, E., 2021. Scaling and responses of extreme hourly precipitation in three climate experiments with a convection-permitting model. Phil. Trans. Roy. Soc. A 379 (2195). https://doi.org/10.1098/rsta.2019.0544.
Liu, Y., Chen, J., Pan, T., Liu, Y., Zhang, Y., Ge, Q., Ciais, P., Penuelas, J., 2020. Global socioeconomic risk of precipitation extremes under climate change. Earth's Future 7. https://doi.org/10.1029/2019EF001331 e2019EF001331.
Lochbihler, K., Lenderink, G., Siebesma, A.P., 2017. The spatial extent of rainfall events and its relation to precipitation scaling. Geophys. Res. Lett. 44, 8629–8636. https://doi.org/10.1002/2017GL074857.
Lyon, B., 2014. Seasonal drought in the Greater Horn of Africa and its recent increase during the March–May long rains. J. Climate 27, 7953–7975. https://doi.org/10.1175/JCLI-D-13-00459.1.
MacKellar N., New, M., Jack, C., 2014. Observed and modelled trends in rainfall and temperature for South Africa: 1960–2010. S. Afr. J. Sci., 110(7/8), 10.1590/sajs.2014/20130353.
Mann, H.B., 1945. Nonparametric tests against trend. Econometrica 13, 245. https://doi.org/10.2307/1907187.
Marani, M., Ignaccolo, M., 2015. A metastatistical approach to rainfall extremes. Adv. Water Resour. 79, 121–126. https://doi.org/10.1016/j.advwatres.2015.03.001.
Marra, F., Borga, M., Morin, E., 2020. A unified framework for extreme sub-daily precipitation frequency analyses based on ordinary events. Geophys. Res. Lett. 47 (18) https://doi.org/10.1029/2020GL090209 e2020GL090209.
Marra, F., Zoccatelli, D., Armon, M., Morin, E., 2019. A simplified MEV formulation to model extremes emerging from multiple nonstationary underlying processes. Adv. Water Resour. 127, 280–290. https://doi.org/10.1016/j.advwatres.2019.04.002.
Masunaga, H., Schroder, M., Furuzawa, F.A., Kummerow, C., Rustemeir, E., Schneider, U., 2019. Inter-product biases in global precipitation extremes. Environ. Res. Lett. 14, 125016 https://doi.org/10.1088/1748-9326/ab5da9.
Miniussi, A., Marani, M., 2020. Estimation of daily rainfall extremes through the metastatistical extreme value distribution: Uncertainty minimization and implications for trend detection. Water Resour. Res. 56, 7. https://doi.org/10.1029/2019WR026535.
Miniussi, A., Marra, F., 2021. Estimation of extreme daily precipitation return levels at-site and in ungauged locations using the simplified MEV approach. J. Hydrol. 603, 126946 https://doi.org/10.1016/j.jhydrol.2021.126946.
Morin, E., Marra, F., Armon, M., 2020. Dryland precipitation climatology from satellite observations. In: Levizzani, V., Kidd, C., Kirschbaum, D., Kummerow, C., Nakamura, K., Turk, F.J. (Eds.), Satellite Precipitation Measurement. Advances in Global Change Research, 69. Springer, Cham. https://doi.org/10.1007/978-3-030-35798-6_19.
Mtewele, Z.F., Xu, X., Jia, G., 2021. Heterogeneous trends of precipitation extremes in recent two decades over East Africa. J. Meteorol. Res. 35, 1057–1073. https://doi.org/10.1007/s13351-021-1028-8.
Myhre, G., Alterskjær, K., Stjern, C.W., Hodnebrog, Ø., Marelle, L., Samset, B.H., Sillmann, J., Schaller, N., Fischer, E., Schulz, M., Stohl, A., 2019. Frequency of extreme precipitation increases extensively with event rareness under global warming. Sci. Rep. 9, 16063. https://doi.org/10.1038/s41598-019-52277-4.
Nasri, B., Tramblay, Y., El Adlouni, S., Hertig, E., Ouarda, T., 2016. Atmospheric predictors for annual maximum daily precipitation in North Africa. J. Appl. Meteor. Climatol. 55 (4), 1063–1076. https://doi.org/10.1175/JAMC-D-14-0122.1.
Nicholson, S.E., Fink, A.H., Funk, C., 2018. Assessing recovery and change in West Africa's rainfall regime from a 161-year record. Int. J. Climatol. 38, 3770–3786. https://doi.org/10.1002/joc.5530.
Nka, B.N., Oudin, L., Karambiri, H., Paturel, J.E., Ribstein, P., 2015. Trends in floods in West Africa: analysis based on 11 catchments in the region. Hydrol. Earth Syst. Sci. 19, 4707–4719. https://doi.org/10.5194/hess-19-4707-2015.
O'Connor, J.C., Dekker, S.C., Stall, A., Tuinenburg, O.A., Rebel, K.T., Santos, M.J., 2021. Forests buffer against variations in precipitation. Glob. Change Biol. 27, 4686–4696. https://doi.org/10.1111/gcb.15763.
O'Gorman, P.A., Schneider, T., 2009. Scaling of precipitation extremes over a wide range of climates simulated with an idealized GCM. J. Climate 22, 5676–5685. https://doi.org/10.1175/2009JCLI2701.1.
Paeth, H., Vogt, G., Paxian, A., Hertig, E., Seubert, S., Jacobeit, J., 2017. Quantifying the evidence of climate change in the light of uncertainty exemplified by the Mediterranean hot spot region. Glob. Planet. Change 151, 144–151. https://doi.org/10.1016/j.gloplacha.2016.03.003.
Panthou, G., Vischel, T., Lebel, T., 2014. Recent trends in the regime of extreme rainfall in the Central Sahel. Int. J. Climatol. 34, 3998–4006. https://doi.org/10.1002/joc.3984.
Papalexiou, S.M., AghaKouchak, A., Foufoula-Georgiou, E., 2018. A diagnostic framework for understanding climatology of tails of hourly precipitation extremes in the United States. Water Resour. Res. 54, 9, 6725–6738. https://doi.org/10.1029/2018WR022732.
Peleg, N., Marra, F., Fatichi, S., Molnar, P., Morin, E., Sharma, A., Burlando, P., 2018. Intensification of convective rain cells at warmer temperatures observed from high-resolution weather radar data. J. Hydrometeor. 19, 715–726. https://doi.org/10.1175/JHM-D-17-0158.1.
Pendergrass, A., 2018. What precipitation is extreme? Science 360, 6393. https://doi.org/10.1126/science.aat1871.
Pfahl, S., O'Gorman, P.A., Fischer, E.M., 2017. Understanding the regional pattern of projected future changes in extreme precipitation. Nature. Clim. Change 7, 423–428. https://doi.org/10.1038/NCLIMATE3287.
Prosdocimi, I., Kjeldsen, T., 2021. Parametrisation of change-permitting extreme value models and its impact on the description of change. Stoch. Environ. Res. Risk Assess. 35, 307–324. https://doi.org/10.1007/s00477-020-01940-8.
Raghavendra, A., Zhou, L., Jiang, Y., Hua, W., 2018. Increasing extent and intensity of thunderstorms observed over the Congo Basin from 1982 to 2016. Atmos. Res. 213, 17–26. https://doi.org/10.1016/j.atmosres.2018.05.028.
Rajulapati, C.R., Papalexiou, S.M., Clark, M.P., Razavi, S., Tang, G., Pomeroy, J.W., 2020. Assessment of extremes in global precipitation products: How reliable are they? J. Hydrometeor. 21 (12), 2855–2873. https://doi.org/10.1175/JHM-D-20-0040.1.
Robinson, A., Lehmann, J., Barriopedro, D., Rahmstorf, S., Coumou, D., 2021. Increasing heat and rainfall extremes now far outside the historical climate. Npj Clim. Atmos. Sci. 4, 51. https://doi.org/10.1038/s41612-021-00212-8.
Samuels, R., Rimmer, A., Alpert, P., 2009. Effect of extreme rainfall events on the water resources of the Jordan River. J. Hydrol. 375, 513–523. https://doi.org/10.1016/j.jhydrol.2009.07.001.
Satgé, F., Defrance, D., Sultan, B., Bonnet, M.P., Seyler, F., Rouché, N., Pierron, F., Paturel, J.E., 2020. Evaluation of 23 gridded precipitation datasets across West Africa. J. Hydrol. 581, 124412 https://doi.org/10.1016/j.jhydrol.2019.124412.
Schär, C., Ban, N., Fischer, E.M., Rajczak, J., Schmidli, J., Frei, C., Giorgi, F., Karl, T.R., Kendon, E.J., Klein Tank, A.M.G., O'Gorman, P.A., Sillmann, J., Zhang, X., Zwiers, F.W., 2016. Percentile indices for assessing changes in heavy precipitation events. Clim. Change 137, 201–216. https://doi.org/10.1007/s10584-016-1669-2.
Sen, P.K., 1968. Estimates of the regression coefficient based on Kendall's tau. J. Amer. Statist. Assoc. 63, 1379–1389. https://doi.org/10.1080/01621459.1968.10480934.
Serinaldi, F., Kilsby, C.G., 2015. Stationarity is undead: Uncertainty dominates the distribution of extremes. Adv. Water Resour. 77, 17–36. https://doi.org/10.1016/j.advwatres.2014.12.013.
Serinaldi, F., Lombardo, F., Kilsby, C.G., 2020. All in order: Distribution of serially correlated order statistics with applications to hydrological extremes. Adv. Water Resour. 144, 103686 https://doi.org/10.1016/j.advwatres.2020.103686.
Sharma, A., Wasko, C., Lettenmeier, D.P., 2018. If precipitation extremes are increasing, why aren't floods? Water Resour. Res. 54 (11), 8545–8551. https://doi.org/10.1029/2018WR023749.
Sun, Q., Zhang, X., Zwiers, F., Westra, S., Alexander, L.V., 2021. A global, continental, and regional Analysis of changes in extreme precipitation. J Climate 34 (1), 243–258. https://doi.org/10.1175/JCLI-D-19-0892.1.
Svensson, C., Jones, D.A., 2010. Review of methods for deriving areal reduction factors. J. Flood Risk Manag. 3 (3), 232–245. https://doi.org/10.1111/j.1753-318X.2010.01075.x.
Taylor, C.M., Belusic, D., Guichard, F., Parker, D.J., Vischel, T., Bock, O., Harris, P.P., Janicot, S., Klein, C., Panthou, G., 2017. Frequency of extreme Sahelian storms tripled since 1982 in satellite observations. Nature 544, 475–478. https://doi.org/10.1038/nature22069.
Taylor, R.G., Todd, M.C., Kongola, L., Maurice, L., Nahozya, E., Sanga, H., Macdonald, A.M., 2013. Evidence of the dependence of groundwater resources on extreme rainfall in East Africa. Nature Clim. Change 3, 374–378. https://doi.org/10.1038/nclimate1731.
Tierney, J.E., Ummenhofer, C.C., deMenocal, P.B., 2015. Past and future rainfall in the Horn of Africa. Sci. Adv. 1 (9) https://doi.org/10.1126/sciadv.1500682.
Tramblay, Y., Somot, S., 2018. Future evolution of extreme precipitation in the Mediterranean. Clim. Change 151, 289–302. https://doi.org/10.1007/s10584-018-2300-5.
Tramblay, Y., Neppel, L., Carreau, J., Sanchez-Gomez, E., 2012. Extreme value modelling of daily areal rainfall over Mediterranean catchments in a changing climate. Hydrol. Process. 25 (26), 3934–3944. https://doi.org/10.1002/hyp.8417.
Tramblay, Y., Villarini, G., Zhang, W., 2020. Observed changes in flood hazard in Africa. Environ. Res. Lett. 15, 1040b5. https://doi.org/10.1088/1748-9326/abb90b.
Vischel, T., Panthou, G., Peyrille, P., Roehrig, R., Quantin, G., Lebel, T., Wilcox, C., Beucher, F., Budiarti, M., 2019. Precipitation extremes in the West African Sahel: recent evolution and physical mechanisms. In: Venugopal, V., Sukhatme, J., Murtugudde, R., Roca, R. (Eds.), Tropical Extremes, Natural variability and trends. Elsevier, ISBN 978-0-12-809248-4. https://doi.org/10.1016/B978-0-12-809248-4.00004-2.

Visser, J.B., Wasko, C., Sharma, A., Natha, R., 2021. Eliminating the "hook" in precipitation–temperature scaling. J. Climate 34, 9535–9549. https://doi.org/10.1175/JCLI-D-21-0292.1.

Wainwright, C.M., Finney, D.L., Kilavi, M., Black, E., Marsham, J.H., 2021. Extreme rainfall in East Africa, October 2019-January 2020 and context under future climate change. Weather 76, 26–31. https://doi.org/10.1002/wea.3824.

Washington, R., Harrison, M., Conway, D., Black, E., Challinor, A., Grimes, D., Todd, M., 2006. African climate change: taking the shorter route. Bull. Amer. Meteor. Soc. 87, 1355–1366. https://doi.org/10.1175/BAMS-87-10-1355.

Wasko, C., Sharma, A., Westra, S., 2016. Reduced spatial extent of extreme storms at higher temperatures. Geophys. Res. Lett. 43, 4026–4032. https://doi.org/10.1002/2016GL068509.

Westra, S., Alexander, L.V., Zwiers, F.W., 2013. Global increasing trends in annual maximum daily precipitation. J. Climate 26, 3904–3918. https://doi.org/10.1175/JCLI-D-12-00502.1.

Williams, A.P., Funk, C., 2011. A westward extension of the warm pool leads to a westward extension of the Walker circulation, drying eastern Africa. Clim. Dyn. 37, 2417–2435. https://doi.org/10.1007/s00382-010-0984-y.

Wilson, P., Toumi, R., 2005. A fundamental probability distribution for heavy rainfall. Geophys. Res. Lett. 32, L14812. https://doi.org/10.1029/2005GL022465.

WMO: State of the climate in Africa 2020. WMO Rep. No. 1275, ISBN 978-92-63-11275-0. https://library.wmo.int/index.php?lvl=notice_display&id=21973#.YZzH6C9aZqs, 2021.

Zhang, X., Zweirs, F.W., Li, G., 2004. Monte Carlo experiments on the detection of trends in extreme values. J. Climate 17, 1945–1952. https://doi.org/10.1175/1520-0442(2004)017<1945:MCEOTD>2.0.CO;2.

Zhou, L., Tian, Y., Myneni, R.B., Ciais, P., Saatchi, S., Liu, Y.Y., Piao, S., Chen, H., Vermote, E.F., Song, C., Hwang, T., 2014. Widespread decline of Congo rainforest greenness in the past decade. Nature 509, 86–90. https://doi.org/10.1038/nature13265.

Ziese, M., Rauthe-Schöch, A., Becker, A., Finger, P., Rustemeier, E., Schneider, U., 2020. GPCC Full Data Daily Version 2020 at 1.0°: Daily land-surface precipitation from rain-gauges built on GTS-based and historic data., 10.5676/DWD_GPCC/FD_D_V2020_100.

Zorzetto, E., Botter, G., Marani, M., 2016. On the emergence of rainfall extremes from ordinary events. Geophys. Res. Lett. 43, 8076–8082. https://doi.org/10.1002/2016GL069445.